A Parametric Model of Cervical Spine Geometry and Posture

Final Report
UMTRI-2017-1

Matthew P. Reed
Monica L.H. Jones

Biosciences Group
University of Michigan Transportation Research Institute

February 2017

A Parametric Model of Cervical Spine Geometry and Posture

Final Report

UMTRI-2017-1

by

Matthew P. Reed
Monica L.H. Jones

University of Michigan Transportation Research Institute

February 2017

REPORT DOCUMENTATION PAGE

Form Approved
OMB No. 0704-0188

1. REPORT DATE *(DD-MM-YYYY)*	2. REPORT TYPE	3. DATES COVERED *(From - To)*
February 2017	Final Report	

4. TITLE AND SUBTITLE

A Parametric Model of Cervical Spine Geometry and Posture

5a. CONTRACT NUMBER
W56HZV-04-2-0001 P00038

5b. GRANT NUMBER

5c. PROGRAM ELEMENT NUMBER

6. AUTHOR(S)

Reed, Matthew P. and Jones, Monica L.H.

5d. PROJECT NUMBER

5e. TASK NUMBER

5f. WORK UNIT NUMBER

7. PERFORMING ORGANIZATION NAME(S) AND ADDRESS(ES)

University of Michigan
Transportation Research Institute

8. PERFORMING ORGANIZATION REPORT

UMTRI-2017-1

9. SPONSORING / MONITORING AGENCY NAME(S) AND ADDRESS(ES)

US Army Natick Soldier Research, Development, and Engineering Center, Natick, MA

10. SPONSOR/MONITOR'S ACRONYM(S)

11. SPONSOR/MONITOR'S REPORT NUMBER(S)
Issued Upon Submission

12. DISTRIBUTION / AVAILABILITY STATEMENT

13. SUPPLEMENTARY NOTES

14. ABSTRACT

Computational models of the cervical spine are useful tools for research on the biomechanics of neck injury and the evaluation of countermeasures. This report describes the development of a parametric model of cervical spine geometry that is intended to provide input to computational modeling. Two-dimensional landmark data describing the outlines of the bones of the cervical spine and important head landmarks were obtained from lateral radiographs of volunteers in a seated posture taken in a previous study. After imputation and a scaling adjustment, principal component analysis was performed on neutral-posture landmark data from 140 men and women with a wide range of age and body size. The first principal component was primarily related to spine curvature, whereas the second was associated with overall size. A regression analysis predicting principal component scores from subject covariates found significant effects of stature, age, and the ratio of sitting height to stature. Sex was not a significant predictor of principal component scores after accounting for overall body size. A three-dimensional bone shape prediction was created using bone geometry from 38 women extracted from CT studies. A principal component analysis performed on each bone level from C1 to C7 demonstrated that the dominant mode of variation was overall size for C2 but not for the other levels. A detailed examination of vertebra dimensions showed that length, width, and height of the vertebrae and the vertebral bodies at C3 through C7 were not correlated. Two methods for generating 3D geometry to match the 2D predictions were created. First, a method was developed to compute the optimal vector of principal component scores such that the side-view projection of landmarks on the 3D bone best matched the 2D targets. Second, a method based on least-squares alignment and uniform scaling was developed. The method based on principal component scores aligned to the landmarks in the 3D dataset with average root-mean-square (RMS) errors below 1 mm, and matched the mesh with average RMS errors less than 2 mm. When aligning to landmarks generate from the 2D model, RMS errors were less than 2 mm. The RMS errors for the scaling method were only slightly larger. Both the PCAR 2D model and the scaling method for generating 3D bone models were implemented in the Python language for use by other researchers.

15. SUBJECT TERMS
Anthropometry, Cervical Spine

16. SECURITY CLASSIFICATION OF:			17. LIMITATION OF ABSTRACT	18. NUMBER OF PAGES	19a. NAME OF RESPONSIBLE PERSON M.P. Reed
a. REPORT	b. ABSTRACT	c. THIS PAGE		43	19b. TELEPHONE NUMBER *(include area code)*
TBD	TBD	TBD			(734)936-1111

ACKNOWLEDGMENTS

This project was funded by the Army Natick Soldier Research, Development, and Engineering Center via the Johns Hopkins Applied Physics Laboratory. We thank Dr. Brian Corner of US Marine Corps (formerly NSRDEC) for his collaboration on this study. We also thank our collaborators from APL, including Katy Carneal and Nathan Drenkow. In addition to leadership and consultation through the project, the APL team supplied the 3D spine geometry that was critical for the 2D-to-3D mapping model.

CONTENTS

ABSTRACT

Computational models of the cervical spine are useful tools for research on the biomechanics of neck injury and the evaluation of countermeasures. This report describes the development of a parametric model of cervical spine geometry that is intended to provide input to computational modeling. Two-dimensional landmark data describing the outlines of the bones of the cervical spine and important head landmarks were obtained from lateral radiographs of volunteers in a seated posture taken in a previous study. After imputation and a scaling adjustment, principal component analysis was performed on neutral-posture landmark data from 140 men and women with a wide range of age and body size. The first principal component was primarily related to spine curvature, whereas the second was associated with overall size.

A regression analysis predicting principal component scores from subject covariates found significant effects of stature, age, and the ratio of sitting height to stature. Sex was not a significant predictor of principal component scores after accounting for overall body size.

A three-dimensional bone shape prediction was created using bone geometry from 38 women extracted from CT studies. A principal component analysis performed on each bone level from C1 to C7 demonstrated that the dominant mode of variation was overall size for C2 but not for the other levels. A detailed examination of vertebra dimensions showed that length, width, and height of the vertebrae and the vertebral bodies at C3 through C7 were not correlated.

Two methods for generating 3D geometry to match the 2D predictions were created. First, a method was developed to compute the optimal vector of principal component scores such that the side-view projection of landmarks on the 3D bone best matched the 2D targets. Second, a method based on least-squares alignment and uniform scaling was developed. The method based on principal component scores aligned to the landmarks in the 3D dataset with average root-mean-square (RMS) errors below 1 mm, and matched the mesh with average RMS errors less than 2 mm. When aligning to landmarks generate from the 2D model, RMS errors were less than 2 mm. The RMS errors for the scaling method were only slightly larger. Both the PCAR 2D model and the scaling method for generating 3D bone models were implemented in the Python language for use by other researchers.

INTRODUCTION

The cervical spine provides a high level of mobility to the head but is vulnerable to injury due to both chronic and acute loading. Computational modeling of the cervical spine (c-spine) and neck has been useful in understanding the influence of both direct and inertial loading on the head and thorax on c-spine kinematics and tissue strains. However, most c-spine models have used geometry from midsize males, and most c-spine geometry data have been extracted from medical images obtained in supine postures rather than postures corresponding to the loading scenarios of interest.

The current work addresses the need for parametric models of c-spine geometry and posture for men and women with a wide range of body size in seated postures with an unsupported head. These postures are typical of people in vehicle environments, including military ground vehicles and aircraft.

The model developed in this work is based on two data sources: (1) a large-scale study of c-spine geometry and posture conducted by UMTRI in the 1970s using lateral radiographs, and (2) c-spine bone geometry extracted by our collaborators at Johns Hopkins Applied Physics Laboratory (APL) using novel techniques developed for the current work (Drenkow et al. 2017).

The methods for 2D model creation are based in large part on previous work at UMTRI on modeling skeletal structures and whole-body surface shapes. A principal component analysis (PCA) was used to explore the principal modes of variation in the dataset. Linear regression was used to test the effects of subject covariates on the size and shape of the c-spine vertebra and to create a predictive model.

A methodology for mapping 3D bone geometry to 2D landmark configurations was adapted from a method previously developed for fitting whole-body shape models to low-resolution scan data. A second method using least-squares fitting to the landmark locations was also tested.

The resulting models were implemented in Python, an open-source programming language. The source code and associated data files will be available for public use following the project.

METHODS

Data Sources

The two-dimensional landmark data used to create the parametric geometry and posture model were obtained from Snyder et al. (1975). A total of 180 men and women with a wide range of age and body size were sat in a laboratory mockup with an unsupported head and horizontally directed vision. Lateral radiographs (Figure 1) were taken in the neutral posture and at maximum flexion and extension. In more recent work (Klinich et al. 2004), the original radiographs were digitized and a large number of landmark locations on the bones were manually extracted. These data have formed the basis for the development of new ways to represent cervical spine posture (Klinich et al. 2012).

Figure 1. Example of a lateral radiograph in the neutral posture from Snyder et al. (1975).

Imputation and Adjustment of Landmark Data

The bone shapes obtained by landmark extraction in the flexed, neutral, and extended postures necessarily differ somewhat within subject. Moreover, some landmarks are missing in the extreme postures. To address this issue, an alignment and imputation procedure was used. The following process was followed for subject and bone:

1. Missing landmarks in the flexed and extended postures were imputed by aligning the neutral-posture configuration using the available landmarks.

2. The landmarks for each bone in the three postures were aligned using generalized Procrustes, which performs a least-squares alignment.

3. The mean landmark configuration was computed.

4. The mean landmark configuration was aligned to the landmark data in each posture using a least-squares method. This aligned mean configuration was used for subsequent analysis.

Due to these steps, no data were missing and the shapes of the bones for each individual were invariant across postures.

Scaling the UMTRI 2D Data

During the process of developing the 3D model, a discrepancy was noted between the dimensions of the 2D model and those obtained from the APL 3D data. Further investigation was conducted to identify the source of the discrepancy. The 2D landmark locations obtained by digitizing the radiographs were originally scaled by reference to an array of beads oriented vertically in each image (see Figure 1). Snyder et al. (1975) data reports that these beads were "one inch" (i.e., 25.4 mm) apart and located on the "midsagittal plane". The analysis by Klinich et al. (2004, 2007) assumed this scaling relationship. However, a closer examination of the images shows that in most cases the images of the beads overlap that of the head, indicating that the beads were placed adjacent to the head, and not in the midsagittal plane. A detailed review of the study documentation did not reveal an alternative location for the beads. Fortunately, the detailed presentation of data in the Snyder report enabled the estimation of a correction factor.

Snyder et al. (1975) reported "segment lengths" based on the distances between "joint centers", defined as the midpoints of the intervertebral spaces, using the tip of the dens as the upper margin of C2. The results were reported separately for men and women. Tables 1 and 2 list the segment lengths for men and women, along with the total, from Snyder et al. (1975). For comparison, comparable lengths were computed in the 2D landmark data, using the mean of the adjacent anterior and posterior vertebral body landmarks as an estimate of the "joint center." Tables 1 and 2 list these along with the corresponding correction factor defined by the relationship.

The comparison to the segment lengths reported by Snyder produces an average scale factor across men and women of 0.820. The regression based on stature, using the 3D landmark data, produces an average of 0.832. Both indicate that the original 2D dataset obtained from the radiographs (Klinich et al. 2004) is approximately 22% too large, on average. Based on this analysis, the 2D landmark data were scaled by 0.820 prior to analysis.

Table 1
Segment Lengths – Male (mm)

	Snyder (in)*	Snyder (mm)	Original 2D	Ratio
C2	1.509	38.32	47.4	0.808
C3	0.7054	17.92	22.5	0.796
C4	0.6895	17.51	21.8	0.803
C5	0.6715	17.06	21.1	0.808
C6	0.6670	16.94	20.8	0.815
C7	0.7215	18.33	19.3	0.950
Total	4.937	125.41	152.9	**0.820**

* Rounded to four digits

Table 2
Segment Lengths -- Female

	Snyder (in)*	Snyder (mm)	Original 2D	Ratio
C2	1.386	35.21	43.2	0.815
C3	0.6207	15.77	19.6	0.804
C4	0.6160	15.65	18.9	0.828
C5	0.6014	15.28	18.5	0.826
C6	0.6000	15.24	19.2	0.794
C7	0.6548	16.63	19.3	0.862
Total	4.478	113.7	138.7	**0.820**

* Rounded to four digits

Parametric 2D Spine Geometry Modeling

Some subjects from the Snyder sample were excluded due to problems with landmark availability. For example, in some flexed and extended scans, insufficient landmarks were in view to fit all of the vertebra segments and head. Out of the original 180 subjects, a total of 140 men and women with complete landmark sets following imputation were retained for analysis. Table 3 lists summary statistics for these subjects.

The 2D spine landmark data were modeled using principal component analysis (PCA) and regression to predict spine size and shape as a function of subject variables. The methods were based on those used in previous studies to model landmark configurations, body shapes, and bone geometries (Li et al. 2015, Klein et al. 2015, Park and Reed 2015). PCA expresses the variance in spine landmark locations in a transformed space in which each subject's landmark coordinates are expressed as a sum of independent linear combinations of coordinates. The

advantages of PCA for this application are that (1) a large percentage of the variance in the data can be expressed using a relatively small number of values, (2) the major modes of variance in spine geometry can be visualized, and (3) the subsequently developed regression models are independent on each principal component (PC).

Table 3
Summary Statistics for 2D Geometry Sample

Women (N=79)	Mean	SD	Min	Max
Stature (mm)	1606	74.9	1448	1840
Age (years)	43.4	19.4	18	74
Men (N=61)				
Stature (mm)	1734	80.7	1520	1899
Age (years)	42.8	20.8	18	74

The coordinates of the spine landmarks in the *neutral* posture were first aligned to a T1 coordinate system with the origin at the anterior superior body landmark and the positive X axis passing through the posterior T1 spinous process landmark, as shown in Figure 2. The mean T1 angle with respect to global horizontal was 3.2 degrees (sd 7.3 degrees), indicating that the T1 spinous process landmark was on average slightly higher than the anterior-superior T1 body landmark. No significant relationships between body dimensions or age and T1 angle were found. The coordinate data for the 122 landmarks were used. Table 4 describes the landmark naming convention. Table 5 lists the landmarks, which are depicted in representative radiographs in Figures 3 and 4. The head landmarks are infraorbitale, tragion, and the anterior and posterior margins of the occipital condyles.

The landmark coordinates were collapsed into a single geometry vector of 244 elements and the PCA was performed on the covariance matrix. A regression analysis was then conducted using sex, stature, age, body mass index (weight in kg divided by the square of stature in meters), the ratio of sitting height to stature, and the interactions between sex and the other variables as potential predictors of principal component (PC) scores. The regression models were assessed with respect to the statistical significance of the predictors and the overall adjusted R^2 values. The regression models with significant predictors were then used to predict PC scores that were used to reconstruct the spine geometry. The resulting landmark configurations represent the mean expected spine geometry given the values of the predictors.

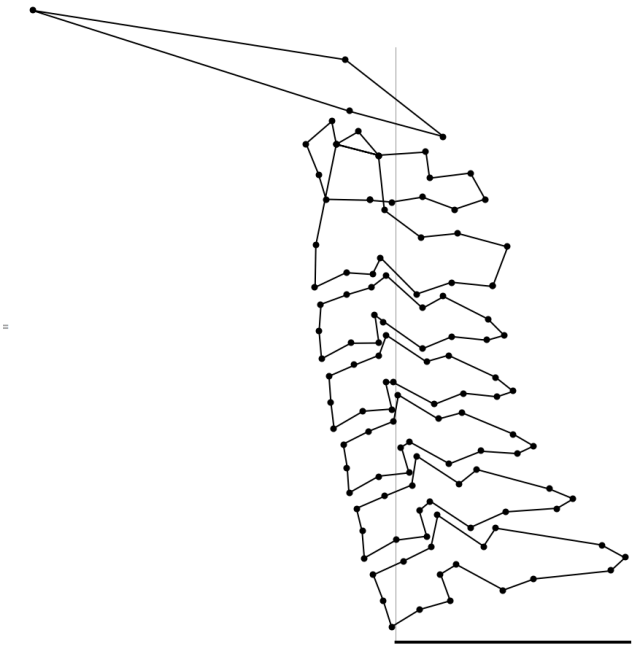

Figure 2. Illustration of landmarks (connected by lines) used in PCA. Horizontal line at the bottom of plot connects anterior-superior body and spinous process landmarks of T1 and defines the coordinate system in which the neutral spine geometry was modeled.

Table 4
Abbreviations in Landmark Names

Abbreviation	Definition
Ant	Anterior
Pos	Posterior
Sup	Superior
Inf	Inferior
Med	Median
SpiPro	Spinous Process
Bod	Body of Vertebra
Den	Dens (C2)
Tub	Tubercle
C1C2	Apparent intersection of the outlines of C1 and C2
Arc	Arch
Can	Canal
Fac	Facet

Table 5
List of Landmarks* Used in PCA

Point Number**	C1 (N=12)	Point Number	C2 (N=16)	Point Number	C3-C7 (N=17)
1	C1_AntSupArc	5	C2_MedAntFce	1	CN_PosInfBod
2	C1_AntTub	6	C2_AntInfBod	2	CN_InfMedBod
3	C1_AntInfArc	7	C2_InfMedBod	3	CN_AntInfBod
4	C1C2_AntInt	8	C2_PosInfBod	4	CN_AntMedBod
18	C1C2_PosInt	9	C2_AntInfFac	5	CN_AntSupBod
19	C1_PosInfArc	10	C2_PosInfFac	6	CN_SupMedBod
20	C1_InfMidArc	11	C2_InfCan	7	CN_PosSupBod
21	C1_InfCan	12	C2_InfSpiPro	8	CN_AntSupFac
22	C1_SpiPro	13	C2_SpiPro†	9	CN_PosSupFac
23	C1_SupCan	14	C2_SupSpiPro	11	CN_PosInfFac
24	C1_SupMidArc	15	C2_SupCan	10	CN_AntInfFac
25	C1_PosSupArc	16	C2_PosSupFac	12	CN_SupCan
		17	C2_AntSupFac	13	CN_InfCan
		26	C2_SupPosDen	14	CN_SupSpiPro
		27	C2_SupMidDen	15	CN_SpiPro
		28	C2_SupAntDen	16	CN_InfSpiPro
				n.s.	CN_PosMedBod

* Abbreviations in landmark names are given in Table 4.
** See Figures 3 and 4.
† Not used in modeling due to missing data for some subjects.
n.s. Not shown.

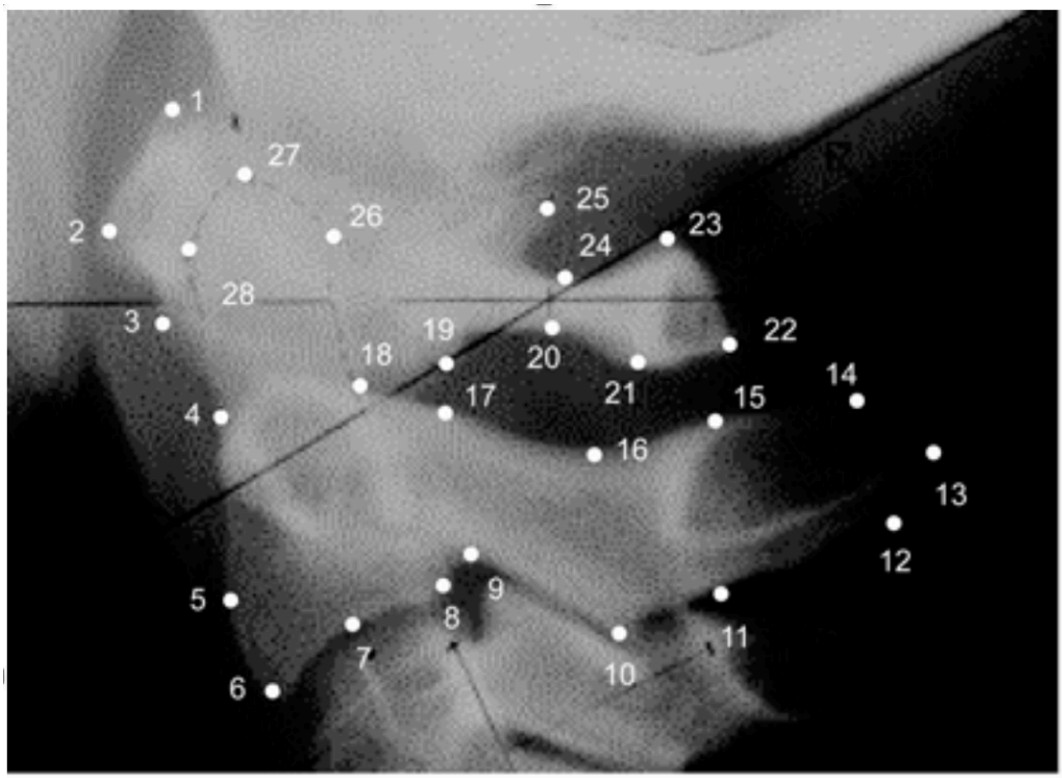

Figure 3. Landmarks digitized on C1 and C2 (Klinich et al. 2004).

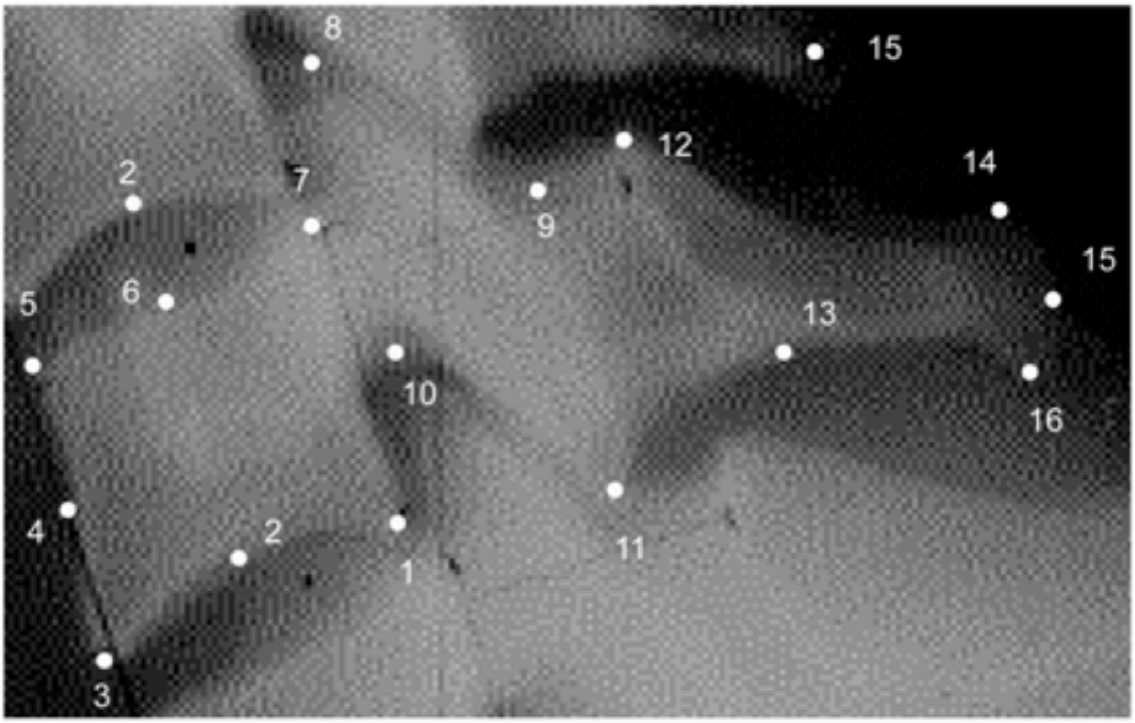

Figure 4. Landmarks digitized on C3 through C7 (Klinich et al. 2004).

Spine Articulation

The three measurement postures provide an opportunity to characterize the spine motion patterns. Ranges of motion can be calculated for each segment based on the differences in orientation of the vertebra between flexed, neutral, and extended postures. Table 6 summarizes range of motion values by level as reported by Snyder et al. (1975). Note that C1 motion with respect to C2 was not quantified. The mean total range of head motion (ROM) with respect to T1 for all subjects in the Snyder dataset was 117 degrees (sd 24 degrees).

Table 6
Total Mean ROM by Motion Segment from Snyder et al. (1975)

Level	ROM (degrees)	Fraction of Head/T1
Head/C1	22.4	0.192
C1/C2	(not measured)	
C2/C3	4.5	0.038
C3/C4	13.2	0.104
C4/C5	23.0	0.197
C5/C6	21.2	0.181
C6/C7	18.7	0.160
C7/T1	15.0	0.128
C2/T1 (sum of above)	94.6	0.809
Head/T1	117	1

With only three postures, it is not possible to characterize the distribution of spine motion for intermediate postures. As an approximation, a spine articulation method was used that distributes motion among the segments according to the fractions of total ROM at each level listed in Table 6. The articulation model is driven by the change from the neutral posture in head orientation relative to T1.

Estimated rotation centers for each segment were taken from Amevo et al. (1991), who used cineradiography to track vertebra motions for neck flexion and extension. The mean rotation centers for each vertebra with respect to the inferior vertebra were reported for C2 to C6. These locations were expressed as fractions of vertebral body height and width. Figure 5 shows the method for establishing a coordinate system equivalent to the one used by Amevo et al. The horizontal axis is established parallel to the line connecting the anterior- and posterior-inferior landmarks by moving the line upward until the axis passes through the inferior median body

landmark. The vertical axis is established perpendicular to the horizontal axis such that it passes through the anterior median body landmark. The height (*h*) and depth (*d*) of the vertebral body are computed from the axes to the lines passing through the superior and posterior median body landmarks.

Table 7 lists the scaled-coordinate locations for each motion center. Figure 6 shows the motion centers on the mean neutral spine. The C7/T1 rotation center was not given by Amevo, and the T1 geometry is not complete in the current dataset. Consequently, the C7/T1 motion center location was estimated with respect to C7 (scaled Z coordinate is negative).

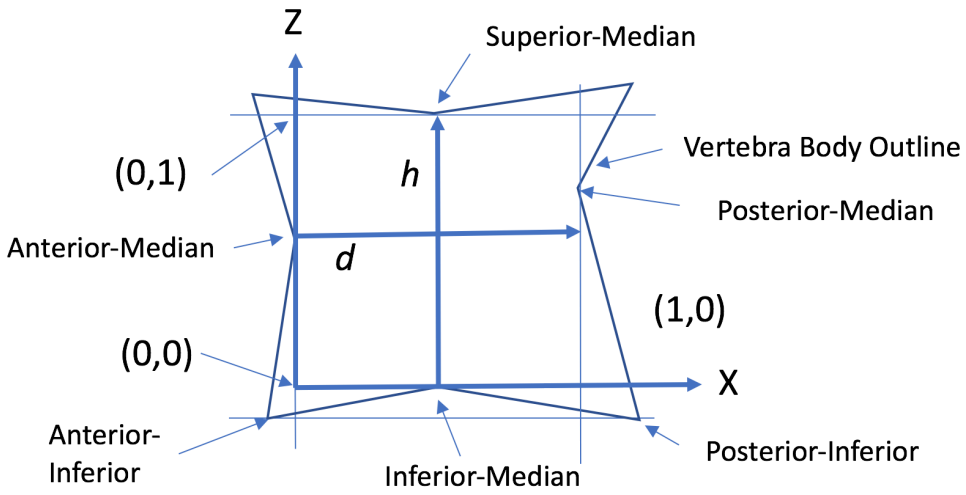

Figure 5. Establishing a coordinate system equivalent to Amevo et al. (1991).

Table 7
C2 through C7 Motion Centers in Scaled* Coordinates from Amevo et al. (1991)

Moving Vertebra	Vertebra Relative to Which Motion Center is Estimated	X Coordinate (scaled)	Z Coordinate (scaled)
C2	C3	0.27	0.36
C3	C4	0.32	0.52
C4	C5	0.36	0.60
C5	C6	0.39	0.78
C6	C7	0.44	0.95
C7†	C7	0.50	-0.05

* Horizontal and vertical coordinates are scaled by the vertebral body depth and height, respectively; see Figure 5.
†Estimated from trend

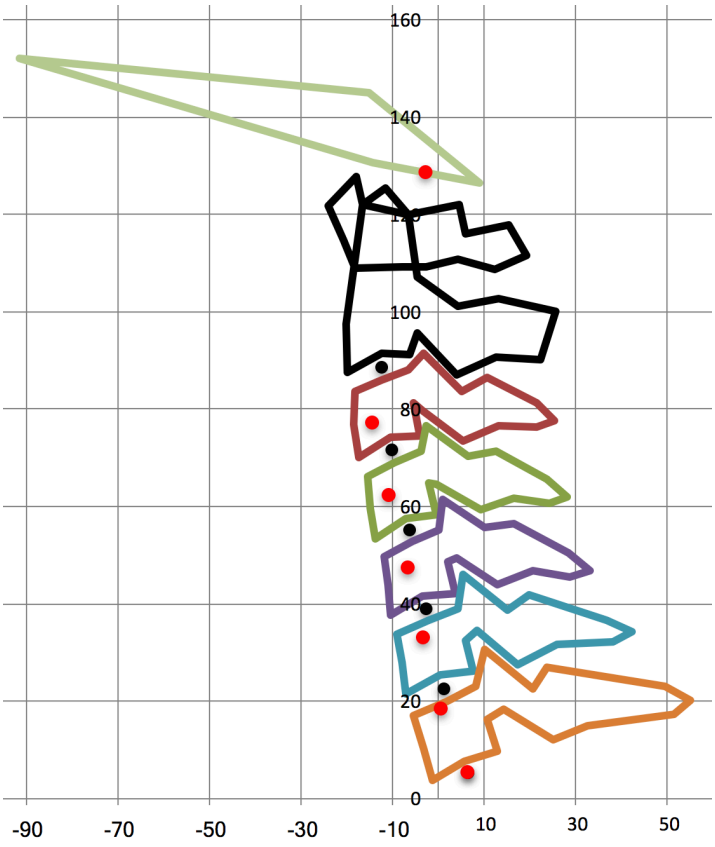

Figure 6. Motion centers (red circles) and intervertebral points (black circles).

Three-Dimensional Vertebra Model

One goal of the project was to develop a method to predict three-dimensional bone shape as a function of the landmark data available in the 2D spine geometry model. Our collaborators at Johns Hopkins Applied Physics Laboratory (APL) developed a pipeline for automated extraction of c-spine bone geometry from CT studies. The methodology for bone extraction is covered in a separate report from APL. In brief, a finite-element mesh was fit to the CT density data using a semi-automated procedure, so each bone is represented by a homologous set of surface node (mesh vertices).

The external surfaces of the bones of 38 female c-spines (C1 through T1) were supplied as homologous meshes. Figure 7 shows an example of three of the spines. Each bone is represented by 996 vertices in a triangular mesh.

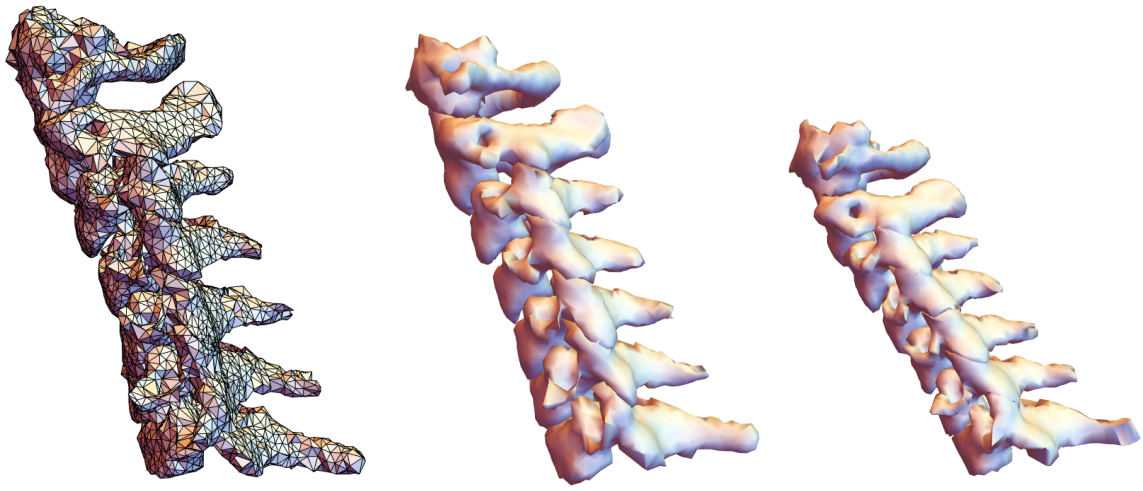

Figure 7. Example spine meshes obtained from CT scans of supine patients. The image on the left shows the individual polygons. The other images are rendered using smooth shading.

Predicting 3D Vertebra Shape from 2D Landmarks: PC Method

The parametric 2D spine model predicts the size and positioning of vertebra but does not predict the full 3D geometry of the bones. To address this issue, a method was developed to link the 3D vertebra geometry to the 2D landmark model to obtain a parametric 3D spine model. The advantages of linking to the 2D model are (1) inclusion of the effects of the stature covariate on bone size and position and (2) representation of the neck posture with an unsupported head.

The method for predicting 3D geometry was as follows:

1. For each bone level:

    a. Align all bones using generalized Procrustes alignment and restore scale.
    b. Compute the mean bone.
    c. Manually identify vertices on the bone corresponding to the 2D landmarks. (This was performed by one individual.)
    d. Perform a PCA on the bone meshes

2. Generate 2D spine geometry prediction for all bones from statistical model as described above.

3. For each bone, compute the 3D bone shape that best fits the selected landmark locations.

    a. Compute the optimal (least squares) alignment of the 2D data to the 3D model using the landmarks listed in Table 4.
    b. Compute the vector of principal component scores that results in the best fit of the bone shape at the selected landmark locations (see below). Iterate to convergence.

c. Align the resulting 3D bone to the 2D spine in position.

An iterative process was used to fit the 3D PCA model for each bone to the selected 2D landmarks. At each iteration, the algorithm took the following steps:

1. Align the 2D and 3D landmarks in the XZ plane using a least-squares fit.
2. Compute the optimal set of values for PC to align the XZ projection of the 3D landmarks with the 2D landmarks (see below for details of this calculation).
3. If iteration has not converged, return to step 1.
4. Apply this vector of PC scores to obtain the full set of surface coordinates for the vertebra.

The optimal vector of PC scores is calculated by exploiting the linear relationship between PC scores and landmark coordinates. Specifically, the individual values in the PC vector represent the rate of change of node coordinates with a unit change in each PC score. Hence, extracting those columns from the PC matrix yields a sensitivity matrix S.

UpdatedPCScores = CurrentPCScores + (CurrentCoordinates-TargetCoordinates).pinv(S)

where pinv is the Moore-Penrose pseudoinverse. This approach calculates the minimum-norm vector of PC scores that will match the coordinates.

To improve the quality of fitting, a new method was developed to limited the range of the calculated PC scores within a range defined by a combination of the range of values in the data and the relative fraction of variance accounted for by the PC. First, a PC weight is assigned based on the relative fraction of variance accounted for in the PCA, with the first PC assigned a value of 1. Second, this weight w_i is used to define a bound for each PC's scores as $\pm w_i\, p\, s$ where s is the standard deviation of scores on PC i (i.e., the eigenvalue) and p is a maximum value. For this analysis p was set to 3, based on a qualitative investigation of fit quality. That is, the maximum score on the first PC is 3 times the eigenvalue; all other PCs are limited more restrictively based on the fraction of variance accounted for by that PC. A similar qualitative investigation determined that the best tradeoff between fit accuracy and smoothness was obtained using 25 PCs.

Table 8
Landmarks Used for 2D->3D Mapping

C1	C2	C3-C7
AntSupArc	AntInfBod	AntInfBod
SpiPro	SupMidDen	AntSupBod
	SupSpiPro	PosSupBod
	InfSpiPro	AntSupFac
	PosInfFac	SupCan
	PosInfBod	SpiPro
		PosInfFac
		PosInfBod

Predicting 3D Vertebra Shape from 2D Landmarks: Scaling Method

The PC-based method provides a good alignment of the 3D landmarks to the 2D targets, but the bone shapes can become somewhat distorted. For some applications, a smoother bone shape with slightly less accurate fitting to the landmark locations might be preferred. Consequently, an alternative method was developed that is computationally simpler and produces smoother bone shapes. The method scales and rotates the mean bone shape to obtain the best (least-squares) alignment to the target landmark locations.

1. Center the target and mean landmark locations by subtracting the respective means.

2. Compute the centroid size (defined as the square root of the sum of squared distances of each point from the origin) and divide the centered coordinates by their respective scales to obtain unscaled landmarks for both target and mean shape. For a matrix P of points $p_i = \{x_i, z_i\}$ the centroid size S is

$$S\ (\text{mm}) = tr(P.\ P^{\mathrm{T}})^{1/2}$$

   where P^{T} indicates the transpose and tr is the trace of the matrix (sum of diagonal elements).

3. Compute the optimal (least-squares) side-view rotation to align the unscaled, centered landmarks from the mean shape to the unscaled, centered target landmarks. The method uses the singular value decomposition (SVD). For centered, unscaled P_1 and P_2, the matrix R to rotate P_2 into P_1 is given by

$$\{U, S, V\} = SVD(P_2^{T}.P_1)$$

$$R = V.U^T$$

4. For each vertex in the mean bone mesh,

    a. subtract the mean of the mean mesh landmark locations
    b. scale by the ratio (target centroid size) / (mean centroid size)
    c. apply the rotation *R* around the Y axis
    d. translate to the target mean

Note that although the translation and rotation of the mean bone mesh occur only in the sagittal plane (side view), the scaling is uniform in 3D. However, the analysis of 3D bone shape showed minimal correlation between sagittal plane dimensions and lateral dimensions (see Results). Consequently, an alternative scaling for lateral dimensions can be applied as a fraction of the sagittal-plane scaling. For example, a scale factor of {1, 0, 1} would apply scaling only the in the sagittal plane.

RESULTS

Parametric 2D Spine Geometry Model in Neutral Seated Posture

The mean 2D spine shape is tabulated in Appendix A. The first 6 PCs accounted for 97% of the variance, as shown in Figure 8. Figure 9 illustrates the first 6 PCs by manipulating the PC by ±3 standard deviations of the associated PC scores while holding the other scores at zero. Somewhat surprisingly, the first PC (65% of variance) is related to posture rather than body size. This demonstrates that the "neutral" neck posture associated with this task condition (seated with self-supported head with forward-oriented vision) is associated with a wide range of spine flexion. The second PC (27%) shows the overall size effect typically seen in PCA of biological structures, but also demonstrates an association between curvature and overall size. The third PC (3%) illustrates variance spine curvature independent of overall spine angle. The remaining PCs account for a total of 5% of variance and each individually less than 1%.

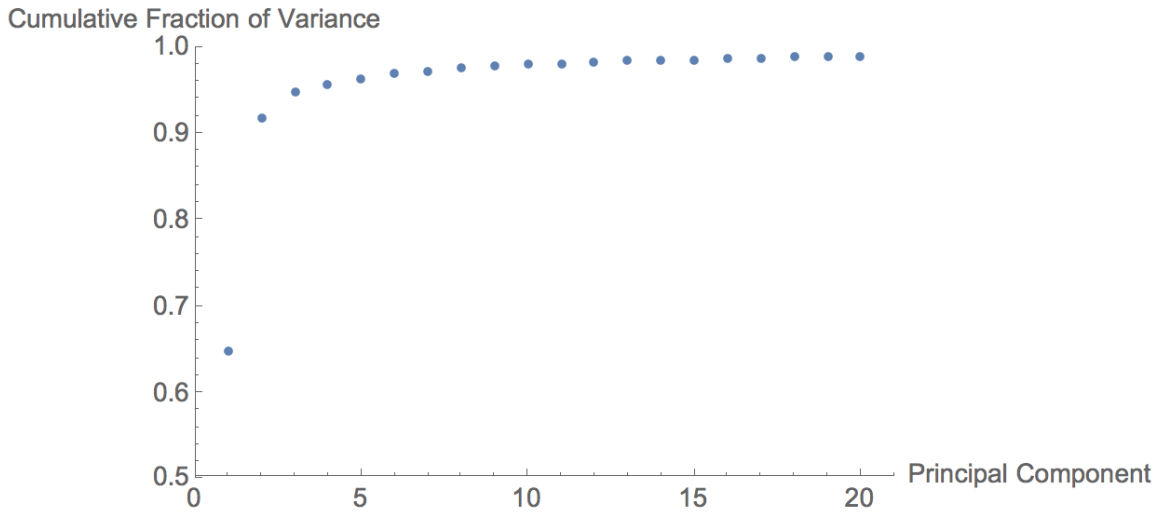

Figure 8. Cumulative percentage of variance associated with principal components.

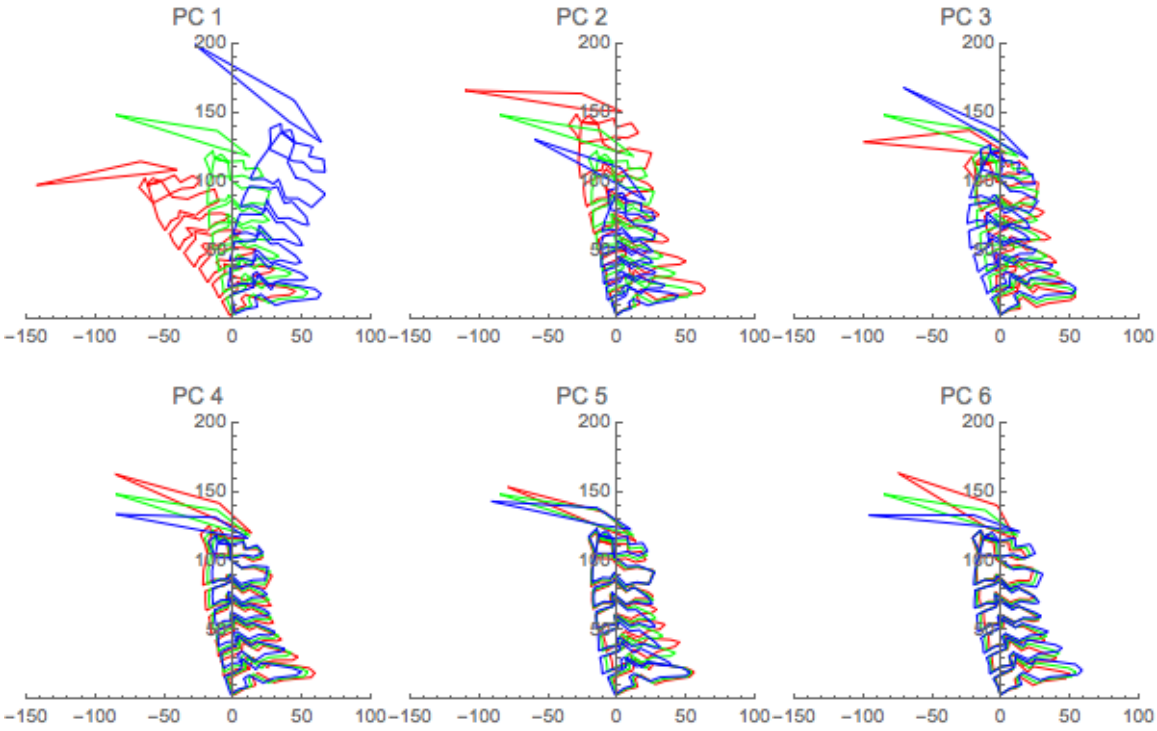

Figure 9. Illustration of PC effects by overlaying mean and geometry obtained by manipulating each PC by ±3 standard deviations of the associated PC scores. Neutral posture is shown in green. Percentage of total variance for PCs 1 through 6: 64.9, 26.9, 3.1, 0.8, 0.7, 0.6

The regression analyses were examined for the first six principal components. In no case was sex or the interaction between sex and another predictor significant in models containing stature. That is, after accounting for overall body size, sex did not have significant effects. Age and the ratio of sitting height to stature (typical value 0.52) were also significant for some PCs. Table 9 shows the significance levels for these predictors along with the adjusted R^2 values for the models. Stature was strongly related to the first two PCs and age was associated with 4 of the first 6. The ratio of siting height to stature was related to the first two PCs. Table 9 shows the signs of the coefficients for each effect. Because the direction of PCs is not unique, the signs are arbitrary except that the same sign for the same PCs indicate parallel effects. For example, on the second PC, which relates primarily to neck length (see Figure 9), the effect of SH/S is in the same direction as that of stature, which is consistent with the individuals having longer torsos having longer necks at a given stature.

Table 9
Significance Test Results in Regression Models Predicting Principal Component (PC) Scores

PC	Stature	Age	Sitting Height/Stature	R^2_{adj}	Fraction of Variance from PCA
1	*** (+)	*** (+)	** (+)	0.24	0.649
2	*** (-)		** (-)	0.52	0.269
3		* (+)		0.02	0.031
4		*** (-)		0.13	0.008
5				n.s.	0.007
6		*** (+)		0.27	0.006

* p<0.05; ** p<0.01; *** p<0.001

The actual geometric effects of the predictors over the ranges of interest are more important than the significance tests. To account for trends that do not reach statistical significance, all three predictors were included for all PCs in subsequent analyses. Figure 10 shows the effects of the stature from 1525 to 1870 mm (5th%ile female to 95th%ile male in ANSUR II (Gordon et al. 2015), 0.500 to 0.546 (5th to 95th%ile for men and women in ANSUR II), and age 20 to 80 years.

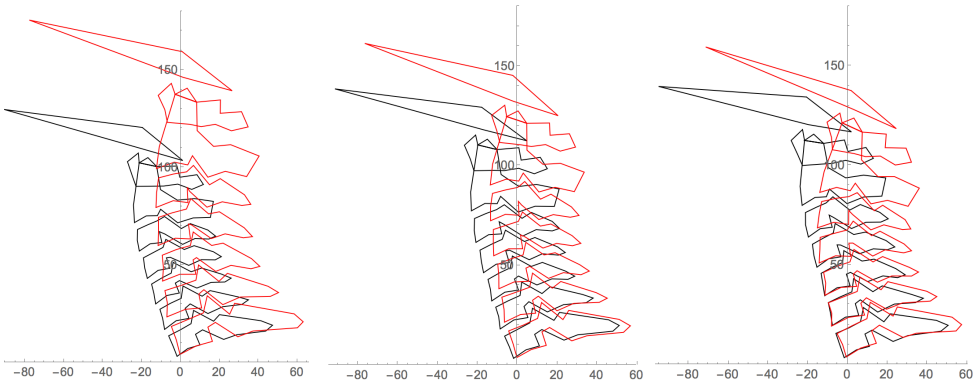

Stature: 1525 to 1870 mm SH/S: 0.50 to 0.55 Age: 20 to 80 years

Figure 10. Illustration of participant covariate effects in neutral posture with the other variables held at mean values (1660 mm, 0.52, 44 years).

Two previous studies have found sex differences in vertebra dimensions using a matched-sample paradigm. Vasavada et al. (2008) measured vertebra dimensions on radiographs obtained from 14 men and 14 women matched closely on stature, erect sitting height, and neck length. Most vertebra depth and height dimensions were slightly smaller for the women (ranging from 0% to 10%), with differences depending on vertebra level and measurement. Vertebra breadth measures were not significantly different. Stemper et al. (2009) conducted a similar study using

samples matched on sitting height (17 males, 11 females) and head circumference (9 males, 18 females). Dimensions were extracted from CT reconstructions. Female dimensions were generally slightly smaller, although the differences were typically less than 10%.

Given these matched-sample findings, the reasons that the current modeling did not show sex effects after accounting for overall body size and age are not clear. Figure 11 shows the result of including sex and interactions between sex, stature, SH/S, and age for all PCs. A small effect of sex is observed, with the predicted geometry being slightly smaller for women. For example, the A-P length of the C7 vertebra is 5% smaller in the predicted female geometry than in the male geometry. Comparing with the population effects in Figure 10, this analysis demonstrates that overall body size (stature and SH/S) have larger effects than sex across the population; that is, most of the differences in vertebra geometry in this data set are attributable to body size rather than sex. The reason for the sex-related spine-length difference in a model that accounts for stature and erect sitting height is unclear. Vadavada et al. (2008) found that a skeletal measure of neck length (vertical distance from C7 spinous process to tragion) was about 5% smaller in a group of women compared to a group of men matched on stature and external neck length, a difference that is consistent with Figure 11.

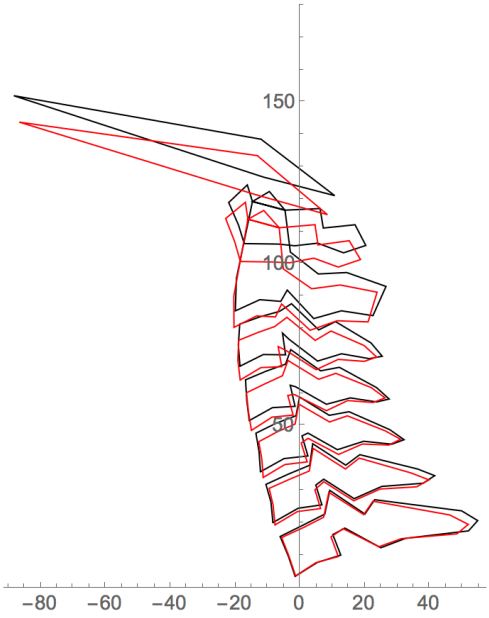

Figure 11. Effect of sex on spine geometry (male=black, female=red), including interactions with stature, SH/S, and age (stature = 1660 mm, SH/S = 0.52, age = 44 yrs).

Model Articulation

Figure 12 shows the result of articulating models representing a midsize male and midsize female to a range of postures. These figures were generated using the Python implementation and a Microsoft Excel viewer (see below). Note that these

postures do not necessarily represent the kinematics of any individual, but at the extremes the model will accurately capture typical ranges of motion.

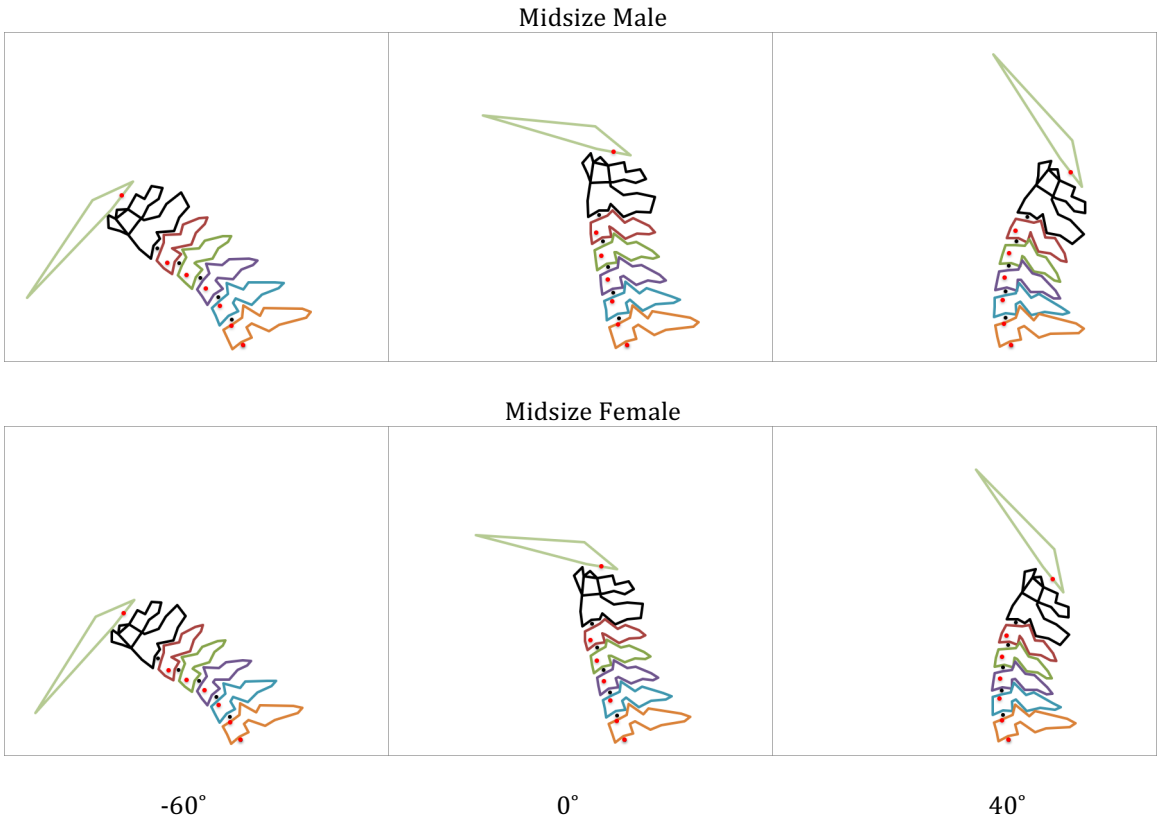

Figure 12. Illustration of spine articulation for change in head angle relative to T1 of -60, 0, and 40 degrees relative to neutral posture.

Covariance of Bone Dimensions

The 3D data provided an opportunity to examine the extent to which bone dimensions are correlated at each vertebral level. Table 10 lists a set of dimensions extracted from each of the bones in the 38 c-spines obtained from CT. The dimensions were measured after each bone was aligned to a consistent coordinate system with the origin at the anterior-inferior body landmark on the midline and the X-axis passing through the posterior-inferior margin (see Figure 2). The vertices corresponding to the vertebra body landmarks in Table 8 were identified on the mean mesh for C3 through C7. The dimensions were subsequently calculated for each bone using the corresponding vertices, under the assumption that the meshes were fully homologous. The overall vertebra dimensions were based on maximum and minimum values on the global axes and could have been measured between different mesh vertices on different bones, depending on the shapes of the bones.

Table 10
Vertebral Dimensions Extracted from 3D Bone Meshes

Dimension	Definition
Vertebra Length	Maximum anterior-posterior dimension
Vertebra Width	Maximum medial-lateral dimension
Vertebra Height	Maximum vertical dimension
Vertebra Body Length	Distance between anterior-inferior and posterior-inferior body landmarks
Vertebra Body Width	Distance between median-inferior left and median-inferior right body landmarks
Vertebra Body Height	Distance between anterior-inferior and anterior-superior body landmarks.

Figures 13 and 14 shows cross plots of vertebra length and width and vertebral *body* length and width. For both pairs of dimensions, no relationships are observed, indicating that the lateral dimensions of the vertebrae are uncorrelated with the lengths (A-P dimensions) in this dataset.

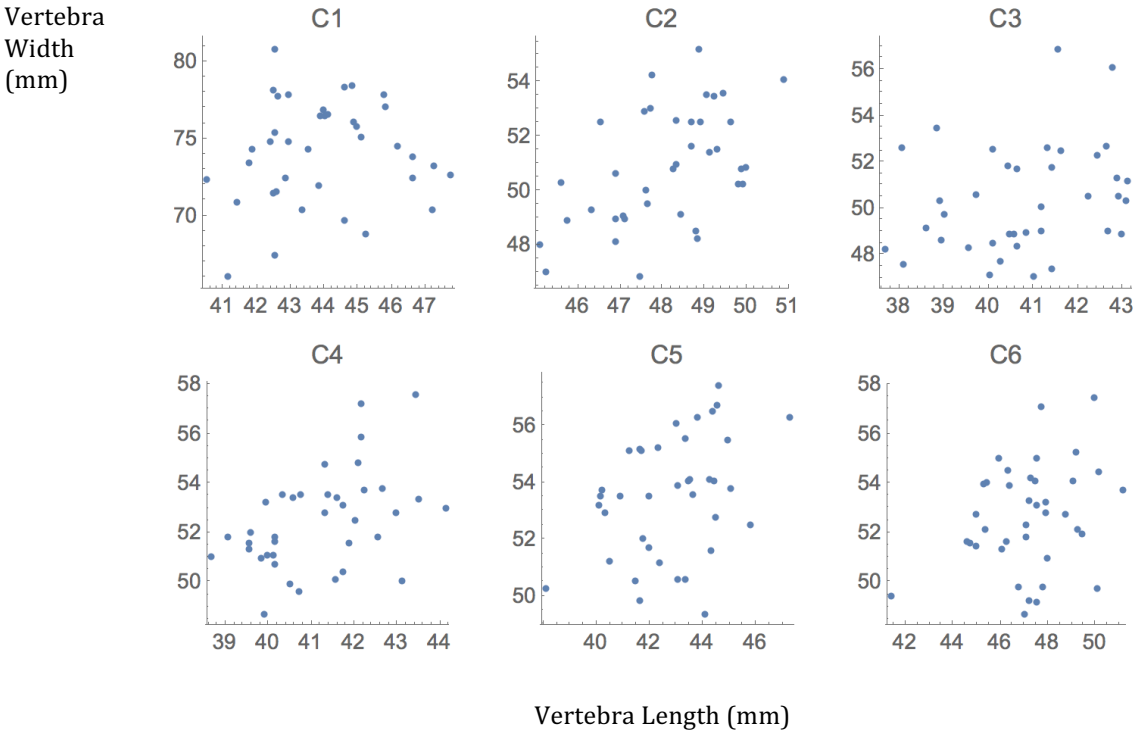

Figure 13. Vertebra length (vertical axis) versus vertebra width (horizontal axis) for bone meshes from 38 women (mm). Note differing scales in subplots.

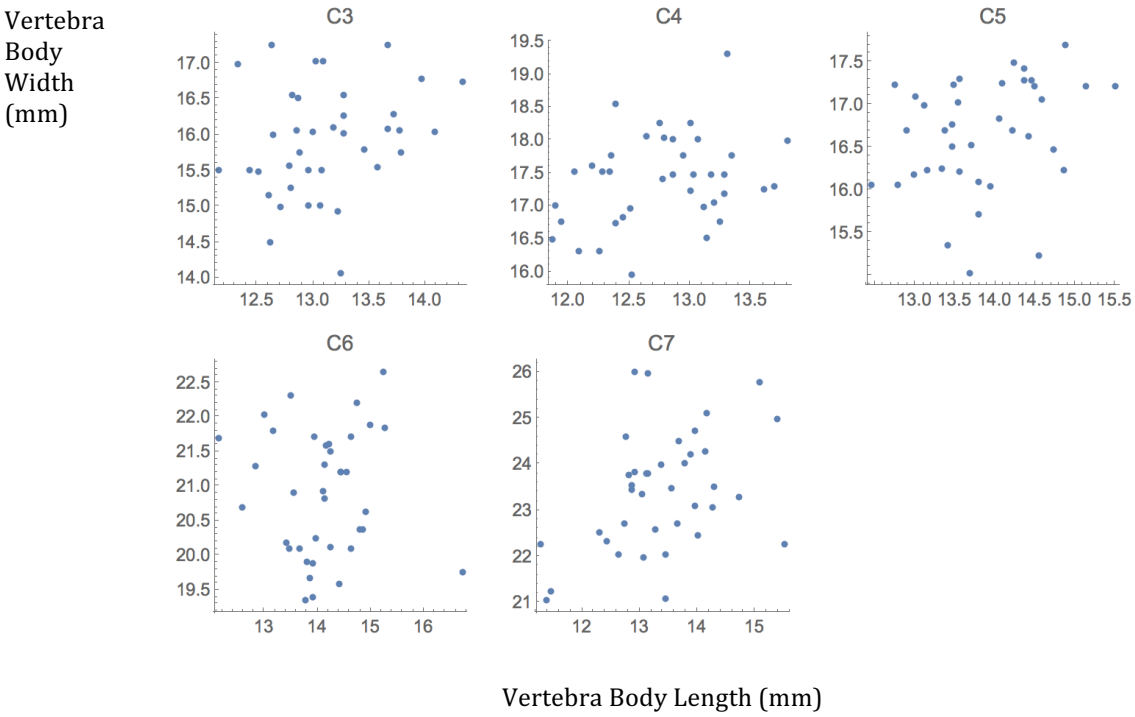

Figure 14. Vertebra body length (vertical axis) versus vertebra body width (horizontal axis) for bone meshes from 38 women (mm). Note differing scales in subplots.

Principal Component Analysis of 3D Bone Shapes

Figures 15 and 16 shows the effects of the first 3 principal components (PCs) for C2 and C4. Each PC affects the location of every mesh vertex, but some trends with respect to the effect of each PC can be noted. For C2, the first PC is related primarily to overall size. PC 2 affects the relative height of the dens, while PC3 is related to the angle of the dens. For C4, the first PC is primarily related to the overall width, while PC 2 has a greater effect on the vertical size. PC 3 is related to the shape of the facets and spinous process.

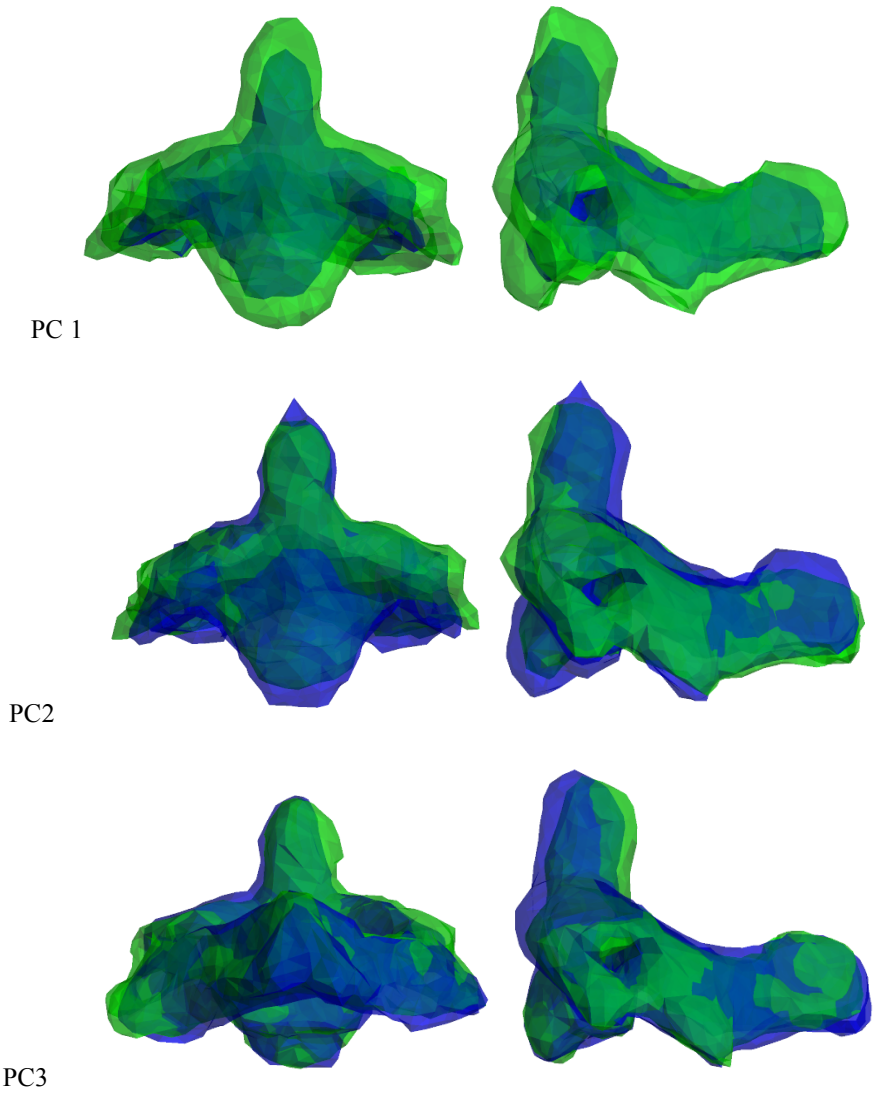

Figure 15. Effects of the first 3 principal components for C2. Overlays show ±3 SD (green and blue) on each of the first 3 components while holding other components at zero.

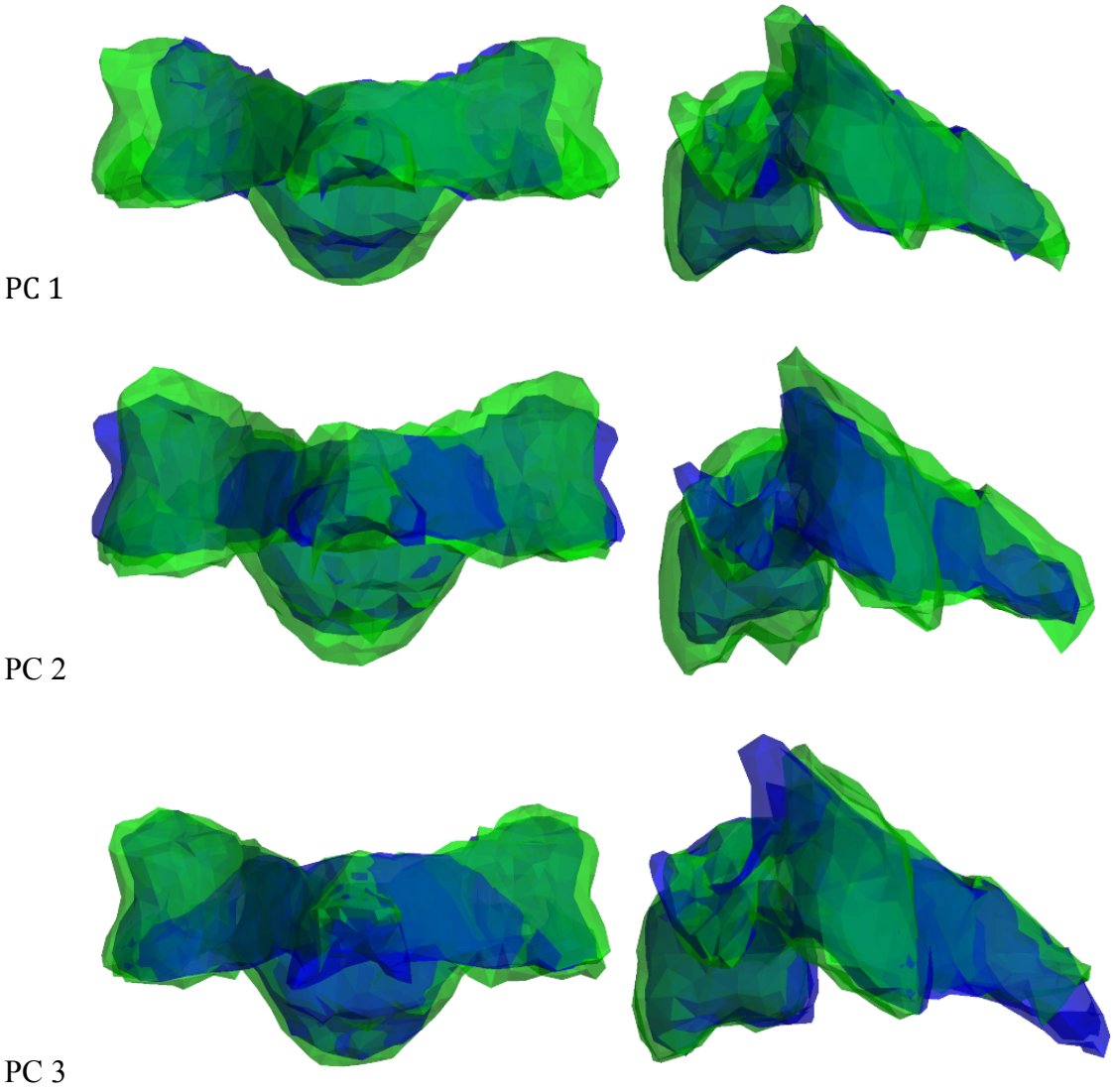

Figure 16. Effects of the first 3 principal components for C4. Overlays show ±3 SD (green and blue) on each of the first 3 components while holding other components at zero.

Results of Fitting 3D Models to 2D Geometry: PC Method

Figure 17 shows the results of fitting the 3D PCA models to the 2D model output for a midsize-female c-spine in several postures. To assess the accuracy of the technique, the procedure was used to fit the PCA models to target points extracted from the original spine data. After fitting, the distance discrepancies between homologous nodes of the mesh were computed and summary statistics across the 996 nodes were calculated. Table 11 lists summary statistics for the fit to the landmarks as well as mean, minimum, and maximum across subjects of the root-mean-square distance discrepancies for each bone. On average, the landmark discrepancy following fitting was less than 0.5 mm. The maximum landmark

discrepancy observed across subjects was under 3 mm. For the mesh, the mean (across subjects) of the RMS error was less than 2 mm for all bones. The maximum discrepancy was largest for C1, at 3.65 mm, but the maximum RMS fitting error for the other bones was less than 2 mm.

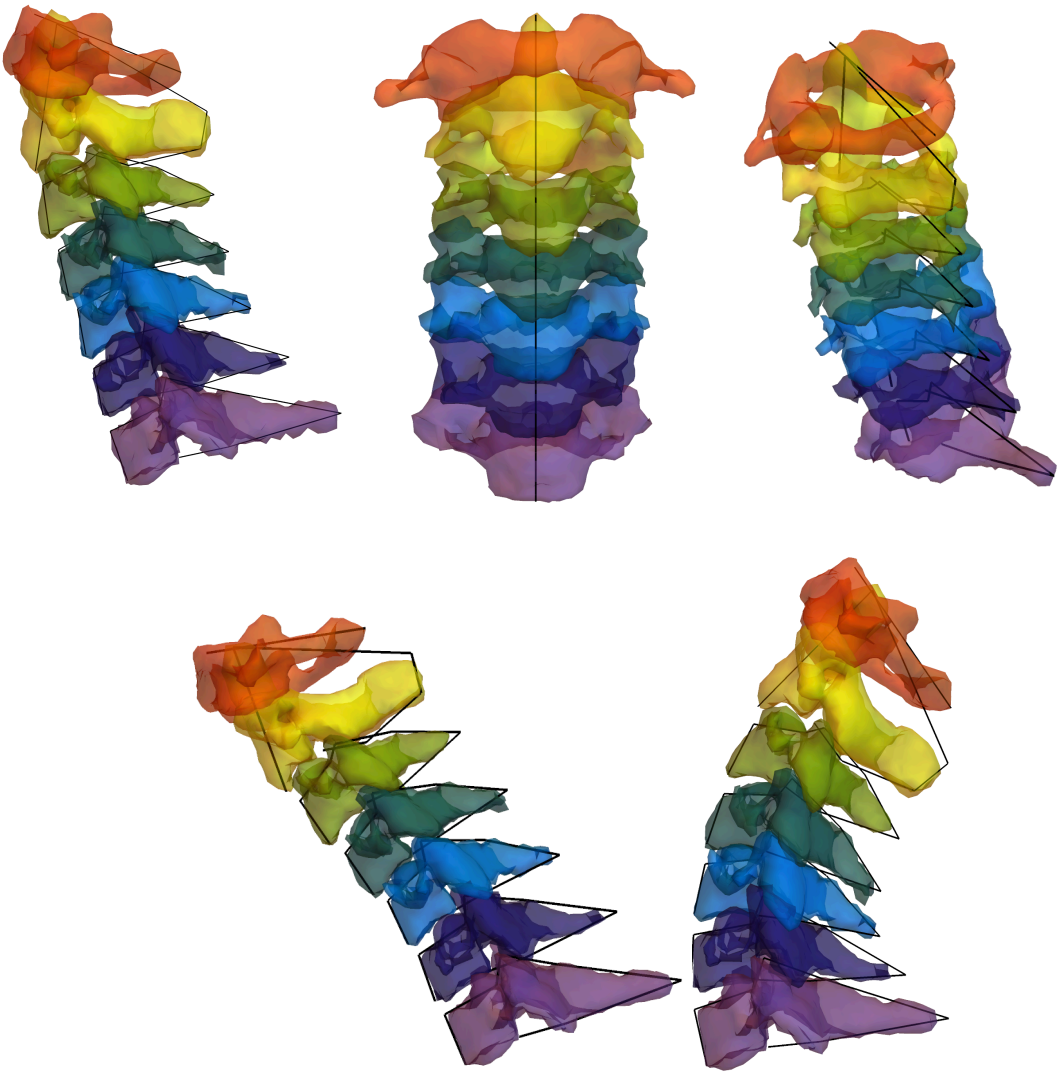

Figure 17. Results of fitting the 3D bone shape to 2D profiles generated from the 2D statistical geometry model. Bones are semitransparent so that lines connecting target landmarks are visible.

Table 11
Fitting Errors* for Landmarks and Mesh: **PCA Method** (mm)

Bone	Landmarks			Mesh		
	Mean	Minimum	Maximum	Mean	Minimum	Maximum
C1	0.28	0.00	0.93	1.90	1.17	3.65
C2	0.56	0.02	2.66	1.13	0.79	1.80
C3	0.34	0.02	2.01	0.93	0.62	1.33
C4	0.34	0.01	1.44	1.00	0.72	1.38
C5	0.45	0.03	2.93	0.98	0.72	1.33
C6	0.36	0.02	1.87	1.02	0.72	1.40
C7	0.46	0.02	2.64	1.25	0.76	1.73

* Root mean square error across 38 subjects (all of the spines used to generate the PC models).

The fitting performance was also assessed by evaluating how closely the fitted landmark locations matched the targets for spine profiles generated from the 2D model. Table 12 shows mean, minimum, and maximum RMS errors in coordinate values for a set of spines generated from the 2D model using statures from 1500 mm to 1750 mm in increments of 50 mm (approximately 5th-percentile female to 95th-percentile female). The RMS errors are somewhat larger than those observed in the CT dataset, likely due to small differences in the placement of the landmarks relative to the bone. Nonetheless, the mean RMS errors are less than 1.5 mm across the 7 bones with maximum RMS errors less than 2 mm.

Table 12
Fitting Errors* for Landmarks for 6 Spine Profiles Generated from 2D: **PC Method** (mm)

Bone	Landmarks		
	Mean	Minimum	Maximum
C1	0.33	0.03	0.82
C2	1.32	1.18	1.49
C3	0.99	0.66	1.32
C4	1.20	0.72	1.59
C5	0.96	0.74	1.10
C6	1.39	0.80	1.84
C7	1.30	1.21	1.38

* Root mean square error across 6 spine profiles generated from the 2D model.

Results of Fitting 3D Models to 2D Geometry: Scaling Method

Table 13 presents the mean, minimum, and maximum RMS errors observed when applying the scaling method to the 3D bone meshes. As expected, both the landmark and mesh errors are larger than those obtained with the PC method, but the mean RMS landmark errors are below 1 mm and the mean RMS mesh errors are 2 mm or less.

Table 14 shows the RMS errors in coordinate values for the same set of 2D spine profiles used for Table 12. Comparing to Table 12, the RMS errors are similar to those obtained using the PC method. This suggests that the PC method is not producing substantially better fit than the simpler scaling model to the landmark predictions from the 2D model.

Table 13
Fitting Errors* for Landmarks and Mesh: **Scaling Method** (mm)

Bone	Landmarks			Mesh		
	Mean	Minimum	Maximum	Mean	Minimum	Maximum
C1	0.00**	0.00**	0.00**	2.01	1.07	3.57
C2	0.79	0.06	2.26	1.22	0.93	1.77
C3	0.69	0.02	2.66	1.08	0.79	1.95
C4	0.69	0.00	2.50	1.15	0.88	1.56
C5	0.82	0.05	3.68	1.18	0.82	2.12
C6	0.83	0.04	2.99	1.27	0.90	2.18
C7	0.94	0.07	3.96	1.50	0.89	2.65

* Root mean square error across 38 subjects.
** Due to the method, the landmark errors for C1, which uses only 2 landmarks for alignment, will always be zero.

Table 14
Fitting Errors* for Landmarks for 6 Spine Profiles Generated from 2D: **Scaling Method** (mm)

Bone	Landmarks		
	Mean	Minimum	Maximum
C1	0.00**	0.00**	0.00**
C2	0.82	0.71	0.99
C3	1.19	1.15	1.24
C4	1.30	1.28	1.33
C5	1.12	1.09	1.18
C6	1.56	1.40	1.73
C7	1.17	1.08	1.29

* Root mean square error across 6 spine profiles generated from the 2D model.
** Due to the method, the landmark errors for C1, which uses only 2 landmarks for alignment, will always be zero.

Python Implementation of 2D Model

To facilitate use of the parametric spine geometry model, a version of the model was implemented in version 3.5 of the Python language (http://python.org/). The Python version includes sex, stature, SH/S, age, and the head angle relative to neutral as inputs. Figure 18 shows a flow chart of the code, which is designed to be executed in a command-line environment. Appendix B contains a user guide for the software. Each time it is executed, the software loads the PC vectors, mean geometry, and regression coefficients for the PCAR model. The input variables are given on the command line. The code generates the landmarks describing each bone shape in the neutral posture, calculates the rotation centers as described above, then articulates the spine using the motion distribution given in Table 6. The resulting bone landmark locations are written to a text file as a series of named points. A simple Microsoft Excel spreadsheet for viewing the results is available with the software. (Figure 12 shows sample graphics from this viewer.)

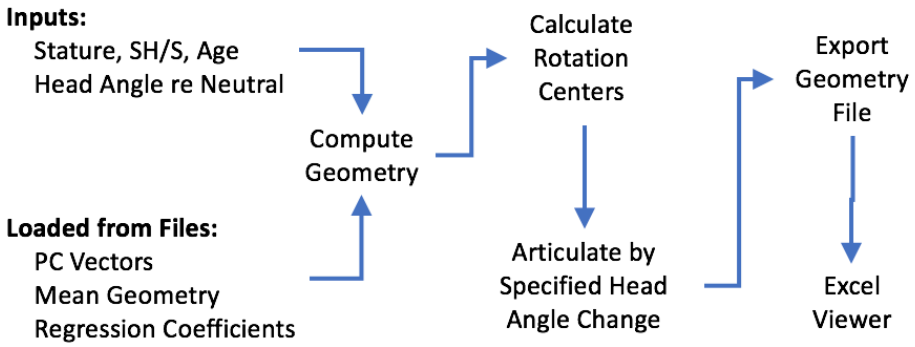

Figure 18. Functional flow of Python implementation of 2D model.

Python Implementation of 3D Model

Because the analysis of the performance of the PC-based and scaling-based methods for 2D-to-3D mapping did not show a strong advantage for the PC-based method, the simpler scaling-based method was implemented in Python. The output file from the 2D model is the input to the software, along with the mean shapes of each of the bones. The Python implementation follows the algorithm laid out above, outputting the scaled and positioned meshes for each bone in OBJ format, a simple text file format that contains vertex coordinates and polygons defined by vertex indices.

DISCUSSION

Two-Dimensional Model

The PCA of 2D landmark locations provided a clear demonstration that "neutral" spine posture is highly variable. Klinich et al. (2012) previously showed this using a spline to quantify curvature, but the current analysis demonstrates that posture dominates overall size in its contribution to the variance in landmark locations across a diverse subject pool. An important conclusion is that modeling aimed at assessing injury risk across a population should focus on posture variability at least as much as geometric variability.

The 2D cervical spine geometry model developed in this work provided an opportunity to test hypotheses about the relationships between overall body size and neck geometry. The primary modes of variation in the spine, quantified by the principal components of the landmark coordinates, did not show significant variation by sex after taking into account overall body size using stature and the ratio of sitting height to stature. Body weight, quantified by body mass index, also did not have significant effects. Age had a small effect including a slightly more extended neck posture with age. An alternative model formulation that included sex predicted a slightly smaller spine for women, after taking into account stature, sitting height, and age, but the effect of sex and the associated interactions were not statistically significant for the first six principal components.

This 2D dataset used in this study is unusual in being obtained from a relatively large, anthropometrically diverse population in a seated posture with a self-supported head. Other 2D data are available, for example the large number of radiographs gathered in the Fels study (Roche 1992), some of which were obtained with a self-supported head. However, the greatest potential for improving the current work is through a larger collection of 3D data obtained from medical CT scans.

Nonetheless, the 2D model has several purposes not yet superseded by other available tools. First, the simple formulation provides an easy way for developers of FE models to scale their cervical geometry accurately to represent individuals with a wide range of body size. For this purpose, the tool augments previous studies that have published distributions of bone dimensions. Importantly, the construction of the model ensures that the set of landmarks generated are internally consistent across a wide range of body size.

Second, and most importantly, the model generates the mean neutral spine configuration for a person sitting in a typical seating posture with an unsupported head. In contrast, nearly all CT studies are obtained with a supine subject with head support, so that the resulting spine curvature is not representative of typical loading cases of interest. One caveat is that the test seat was constructed using simple rigid surfaces, with a seat back at 19 degrees to vertical. However, other studies have

quantified the trends in head and thorax orientation with changes in seat back angle (e.g., Reed and Ebert 2013; Park et al. 2016); these may be used to adjust the predicted postures. Another limitation for modeling applications is that the data do not take into account the effects of head-supported mass on posture.

A simple articulation model was implemented based on previously published segment rotation centers. Initially, the flexed and extended posture data were examined to determine if the motion centers could be calculated reliably. The results, however, were found to be highly variable and ultimately were discarded in favor of the literature values.

The utility of the articulation model is somewhat limited because the motion distribution is constant, which is not a realistic assumption at the limits of movement. The articulation will be most useful for making small changes to account for different seating configurations, such as more-upright or more-reclined seating postures. Nonetheless, given the wide range of spine curvatures in "neutral" postures, any discrepancies in spine curvatures obtained by this method will be small compared with the population variance. Importantly, this articulation model should not be taken to be representative of actual human *movement*.

Three-Dimensional Bone Shape Modeling

The analysis of bone shapes extracted from CT showed several surprising findings. First, the primary mode of variation for C3-C7 was not overall size, but rather a more complex relationship between size and shape. Second, consistent with that finding but more directly relevant for modeling, the overall length, width, and height of the bones were essentially uncorrelated. The same was true of the vertebral body, where no important scaling relationships were observed. This finding is limited by the relatively small and homogeneous sample (spines from 38 women), but even with that caveat the data strongly suggest that the major dimensions of the spine at the level of individual bones are not highly correlated.

For comparison, the 2D model shows a general scaling of the whole spine and the individual vertebra with overall body size (increased stature or sitting height). The 3D analysis suggests that the lateral dimensions likely are only weakly correlated with the overall size, at least for women. This somewhat surprising finding should be confirmed with a larger and more diverse sample. Nonetheless, it is consistent with the finding from the 2D landmark analysis of considerable idiosyncrasy in spine shape across individuals.

A novel method for generating 3D bone shapes from the 2D data was developed based on a PC fitting technique that generates a 3D mesh such that a set of landmarks on the 3D bone is closely aligned with the 2D profile. The technique demonstrated relatively small RMS errors for both the landmarks and mesh when fitting the original 3D dataset, and small RMS errors for fitting landmarks generated from the 2D model for a range of stature.

The method was developed under the assumption that a substantial amount of the lateral size and shape of the bones would be predictable from the 2D profile. In fact, as noted above, lateral dimensions are essentially uncorrelated with profile dimensions in this 3D dataset. Consequently, the lateral dimensions of 3D spines generated by this method are similar across a range of neck lengths.

The 2D-to-3D mapping method generates a 3D model that closely corresponds to the predictions of the 2D model, but given the findings regarding bone shape variability, some simpler scaling methods might work similarly well. For example, the mean bone shape could be scaled in 3 dimensions to match the target vertebra size and aligned to the 2D predictions.

Alternative 3D Model Generation Methods

With a larger dataset, a number of alternative methods of generating a parametric 3D neck model are available.

1. A PCAR model of the whole spine can be created using subject covariates, such as sex, stature, and sitting height as predictors. However, sitting height is not commonly available in patient database from which CT scans are extracted.

2. The c-spine length can be used as a size variable to predict the 3D shape, where the length is generated from the 2D model.

3. Because the data show that c-spine width is unrelated to height and depth, a geometric model of the c-spine can be scaled in side view using simple relationships based on the 2D model. For example, the vertebral height and anterior-posterior length could be used to perform affine scaling. This should produce results similar to the least-squares scaling method developed in the current work.

A central challenge in any landmark-based morphing method is finding truly homologous points. The larger landmark errors associated with fitting the 3D PCA model to 2D model outputs, compared with fitting to homologous points from the 3D dataset, indicates that the landmarks identified on the 3D model are not completely homologous. However, the differences are generally less than a millimeter, suggesting that only small improvements would be realized.

Limitations and Future Work

The accuracy of the 2D model is limited by the challenges in accurately and consistently locating landmarks on the radiographs. Issues relating to this manual digitization process are discussed in Klinich et al. (2004) and in the original Snyder et al. (1975) report.

The current analysis uncovered a scaling problem with the digitization reported in Klinich et al. (2004). The correction applied a constant scaling factor that was

assumed to be appropriate for all subjects. The resulting model prediction using mean female anthropometry was similar in size to the mean 3D spine size, but it is possible that variable scaling factors were used in the original Snyder dataset. These would only affect the current analysis if the true scaling was correlated with one or more of the covariates. However, no indication of that is evident in either the Snyder et al. documentation or the data analysis.

The articulation method provides a reasonable way of adjusting postures around the neutral posture, and produces reasonable estimates at the extremes, due to the use of full flexion/extension range-of-motion to define the distribution of motion. However, the kinematics should not be taken to be representative of the average spine motion between postures for any individual.

The 3D analysis was based on relatively few subjects (38 women). A larger dataset would have provided more confidence in the outcome of the PCA on bone shapes and may have improved the performance of the PC-based fitting method. However, the scaling method, which uses only the average bone shape, would not be improved by the addition of more data.

Future work should include the analysis of 3D data from a wider pool of subjects, including an equal number of men. The observations concerning the lack of correlation among vertebra dimensions should be verified using a larger, more diverse sample.

REFERENCES

Amevo, B., Worth, D., and Bogduk, N. (1991). Instantaneous axes of rotation of the typical cervical motion segments: a study in normal volunteers. *Clinical Biomechanics*, 6:111-117.

Drenkow, N., Pyles, C., Kuo, N., Harrigan, T., Thawait, G., Fritz, J., Carneal, C. (2017). *Improved Head-Neck Finite Element Model for Dynamic Head Impact Simulation.* Technical Report. Johns Hopkins University Applied Physics Laboratory.

Li, Z., Park, B-K, Liu, W., Zhang, J., Reed, M.P., Rupp, J.D., Hoff, C.N., and Hu, J. (2015). A statistical skull geometry model for children 0-3 years old. *PLOS One*, 10(5). 10.1371/journal.pone.0127322

Klein, K.F., Hu, J., Reed, M.P., Hoff, C.N., and Rupp, J.D. (2015). Development and validation of statistical models of femur geometry for use with parametric finite element models. *Annals of Biomedical Engineering,* 43(10): 2503-2514. 10.1007/s10439-015-1307-6

Park, B-K and Reed, M.P. (2015). Parametric body shape model of standing children ages 3 to 11 years. *Ergonomics*, 58(10):1714-1725. 10.1080/00140139.2015.1033480

Klinich, K.D., Ebert, S.M., Van Ee, C.A., Flannagan, C.A., Prasad, M., Reed, M.P., and Schneider, L.W. (2004). Cervical spine geometry in the automotive seated posture: variations with age, stature, and gender. *Stapp Car Crash Journal*, 48:301-330.

Klinich, K.D., Ebert, S.M., Reed, M.P. (2012). Quantifying cervical spine curvature using Bézier splines. *Journal of Biomechanical Engineering,* 11(4): 114503-114508. 10.1115/1.4007749

Gordon, C.C., Blackwell, C.L., Bradtmiller, B., Parham, J.L., Barrientos, P., Paquette, S.P., Corner, B.D., Carson, J.M., Venezia, J.Z., Rockwell, B.M., Mucher, M., and Kristensen, S. (2015). 2012 *Anthropometric Survey of U.S. Army Personnel: Methods and Summary Statistics.* Technical Report NATICK/TR-15/007. U.S. Army Natick Soldier Research, Development and Engineering Center Natick, Massachusetts.

Park, J., Ebert, S.M., Reed, M.P., and Hallman, J.J. (2016). A statistical model including age to predict passenger postures in the rear seats of automobiles. *Ergonomics*, 59(6): 796-805, 10.1080/00140139.2015.1088076

Reed, M.P. and Ebert, S.M. (2013). *The Seated Soldier Study: Posture and Body Shape in Vehicle Seats.* Technical Report 2013-13. University of Michigan Transportation Research Institute, Ann Arbor, MI.

Roche, A. F. (1992). *Growth, Maturation and Body Composition: The Fels Longitudinal Study 1929-1991*. Cambridge University Press.

Snyder, R. G., Chaffin, D. B., and Foust, D. R. (1975). *Bioengineering study of basic physical measurements related to susceptibility to cervical hyperextension-hyperflexion injury.* Final report UM-HSRI-BI-75-6, University of Michigan Transportation Research Institute, Ann Arbor, MI.

Stemper, B.D., Derosia, J.J., Yoganandan, N., Pintar, F.A., Shender, B.S., and Pasko, G.R. (2009) Gender dependent cervical spine anatomical differences in size-matched volunteers. *Biomed Sci Instrum*, 45:149-154.

Vasavada, A.N., Danarajb , J., and Siegmund, G.P. (2008). Head and neck anthropometry, vertebral geometry and neck strength in height-matched men and women. *Journal of Biomechanics*, 41:114-121.

APPENDIX A

Mean 2D Spine Landmark Configuration (mm)

Abbreviations:

Ant	Anterior
Pos	Posterior
Sup	Superior
Inf	Inferior
Med	Median
SpiPro	Spinous Process
Bod	Body of Vertebra
Den	Dens (C2)
Tub	Tubercle
C1C2	Apparent intersection of the outlines of C1 and C2
Arc	Arch
Can	Canal
Fac	Facet

The origin is the anterior-superior body landmark on T1 (T1_ AntSupBod). The X axis is positive from T1_ AntSupBod to the T1 spinous process landmark (T1_SpiPro)

Landmark	X	Z
C2_SupAntDen	-14.1	117.2
C1_AntSupArc	-15.1	122.6
C1_AntTub	-21.2	117.4
C1_AntInfArc	-18.2	110.2
C1C2_AntInt	-16.5	104.3
C1C2_PosInt	-6.2	104.0
C1C2_PosInt	-6.2	104.0
C1_PosInfArc	-1.0	103.6
C1_InfMidArc	6.2	104.8
C1_InfCan	13.9	101.9
C1_SpiPro	21.0	104.3
C1_SupCan	17.5	110.4
C1_SupMidArc	7.9	109.2
C1_PosSupArc	7.0	115.4
C2_SupPosDen	-4.1	114.6

C2_SupAntDen	-14.1	117.2
C2_MedAntFac	-18.9	93.5
C2_AntInfBod	-19.0	83.5
C2_InfMedBod	-11.8	87.0
C2_PosInfBod	-5.6	86.6
C2_AntInfFac	-3.6	90.5
C2_PosInfFac	4.9	81.9
C2_InfCan	13.1	84.7
C2_InfSpiPro	22.7	83.7
C2_InfSpiPro	22.7	83.7
C2_SupSpiPro	26.3	93.0
C2_SupCan	14.5	96.2
C2_PosSupFac	5.8	95.3
C2_AntSupFac	-2.8	101.7
C2_SupPosDen	-4.1	114.6
C2_SupPosDen	-4.1	114.6
C2_SupMidDen	-8.9	120.2
C2_SupAntDen	-14.1	117.2
C3_AntInfBod	-17.5	66.7
C3_AntMedBod	-18.1	73.1
C3_AntSupBod	-17.6	79.5
C3_SupMedBod	-11.6	81.8
C3_PosSupBod	-5.9	83.5
C3_AntSupFac	-2.2	86.3
C3_PosSupFac	6.3	78.6
C3_SupCan	11.2	81.4
C3_SupSpiPro	21.6	76.1
C3_SpiPro	25.4	72.2
C3_InfSpiPro	21.5	71.1
C3_InfCan	13.1	71.9
C3_PosInfFac	6.2	69.1
C3_AntInfFac	-2.9	75.5
C3_PosMedBod	-5.0	77.0
C3_PosInfBod	-4.0	70.4
C3_InfMedBod	-10.7	70.4
C4_AntInfBod	-14.6	50.4
C4_AntMedBod	-15.3	56.5
C4_AntSupBod	-15.8	62.6
C4_SupMedBod	-9.8	65.2
C4_PosSupBod	-4.0	67.5

C4_AntSupFac	-2.3	72.3
C4_PosSupFac	7.1	66.0
C4_SupCan	12.3	67.5
C4_SupSpiPro	23.4	62.4
C4_SpiPro	27.6	59.0
C4_InfSpiPro	23.8	57.8
C4_InfCan	15.7	58.6
C4_PosInfFac	9.0	56.0
C4_AntInfFac	-0.7	61.2
C4_PosMedBod	-2.5	61.2
C4_PosInfBod	-1.0	54.9
C4_InfMedBod	-7.8	54.4
C5_AntInfBod	-11.1	35.1
C5_AntMedBod	-11.5	41.1
C5_AntSupBod	-12.4	46.6
C5_SupMedBod	-6.5	49.6
C5_PosSupBod	-0.6	52.0
C5_AntSupFac	0.6	58.2
C5_PosSupFac	9.9	52.5
C5_SupCan	15.5	54.0
C5_SupSpiPro	27.6	49.0
C5_SpiPro	32.4	46.2
C5_InfSpiPro	28.6	44.4
C5_InfCan	20.0	44.9
C5_PosInfFac	12.6	42.0
C5_AntInfFac	3.2	47.1
C5_PosMedBod	1.3	45.9
C5_PosInfBod	3.0	39.9
C5_InfMedBod	-4.1	39.1
C6_AntInfBod	-7.5	19.8
C6_AntMedBod	-8.0	26.0
C6_AntSupBod	-9.3	31.5
C6_SupMedBod	-2.6	34.4
C6_PosSupBod	3.7	37.0
C6_AntSupFac	4.8	43.9
C6_PosSupFac	14.9	37.3
C6_SupCan	19.0	40.6
C6_SupSpiPro	36.2	36.0
C6_SpiPro	41.7	33.7
C6_InfSpiPro	37.9	31.5

C6_InfCan	25.7	30.7
C6_PosInfFac	17.5	27.0
C6_AntInfFac	8.1	33.2
C6_PosMedBod	5.5	31.0
C6_PosInfBod	7.2	24.9
C6_InfMedBod	-0.1	24.0
C7_AntInfBod	-1.1	3.6
C7_AntMedBod	-3.0	9.8
C7_AntSupBod	-5.4	15.8
C7_SupMedBod	1.8	19.1
C7_PosSupBod	8.2	22.3
C7_AntSupFac	9.8	29.9
C7_PosSupFac	20.6	22.6
C7_SupCan	23.4	26.8
C7_SupSpiPro	48.4	22.9
C7_SpiPro	53.9	19.9
C7_InfSpiPro	50.5	16.8
C7_InfCan	32.5	14.9
C7_PosInfFac	25.3	12.3
C7_AntInfFac	14.2	18.3
C7_PosMedBod	10.5	16.0
C7_PosInfBod	12.8	9.7
C7_InfMedBod	5.6	7.7
Tragion	-11.9	137.1
Infraorbitale	-85.6	148.7
AntOccCon	-10.9	125.0
PosOccCon	11.2	119.0

APPENDIX B
User Guide to Software Implementation

UMTRI Parametric C-Spine Model

Software for generating 2D and 3D cervical spine bone geometry
as a function of anthropometry and posture.

Author: mreed@umich.edu

Revision Date: 2017-02-25

****

Python version 3.x is required; tested with Python version 3.5.

The numpy library is required.

****

```
>>> from CSpine2DPCAR import *

# anthro.FEMALE and anthro.MALE are defined as 1 and -1, respectively


# shs = sitting height / stature

>>> target_anthro = anthro(anthro.FEMALE, stature=1650, age=45, shs=0.52)

>>> pcar = PCARSpine2D()

>>> pcar.predict(target_anthro, delta_head_angle=-30)

# delta head angle from neutral in degrees; negative is flexion
```

The predict() methods generates a spine using the PCAR model, articulates the model according to the delta_head_angle, then writes the model to a file "SpineOut.tsv" that contains named points.

Opening SpineOut.tsv in Excel will automatically update the plot in ViewSpine.xlsx.

The PCARSpine2D.predict() method can also be called with keyword arguments:

>>> pcar.predict(sex=anthro.FEMALE, stature=1750, age=45, delta_head_angle=20)

or with a list of anthro:

>>> pcar.predict(anthro=[1, 1750, 0.52, 45], delta_head_angle=20) # sex: -1=male, 1=male

The module can also be run from the command prompt with the anthro and posture as command-line arguments

$ python CSpine2DPCAR.py 1 1650 0.52 20 0

Note all five arguments (sex, stature, shs, age, and delta head angle) must be supplied. If none is supplied, a midsize female spine is generated in the neutral posture.

A location parameter can be added to the predict() call to translate and rotate the model. Using the argument location='C7' (or other level up to C2) will place the anterior-inferior margin of the body at the origin and align the inferior surface of the body with the global x axis. Alternatively, enter a location and angle, e.g., [[40, 40], 30] will translate the model by [40, 40] and rotate 30 degrees clockwise. The segment positions and orientations are written at the end of the landmark file.

Running CSpine2DPCAR from the command line (executing the module) will automatically run CSpine3DFitting on the result.

****

CSpine3DFitting.py

Usage:

>>> from CSpine3DFitting import *

>>> bm = BoneMapper()

The file SpineOut.tsv residing in the output directory is read. The 3D geometry in the data directory is mapped to the 2D geometry and output as OBJ and landmark files. The OBJ files can be read in meshlab and many other graphics packages.

Alternatively, from the command line

$ python CSpine3DFitting.py

The output directory is expected to contain a file called SpineOut.tsv containing the 2D landmarks.

An alternative file can be supplied on the command line:

$ python CSpine3DFitting.py AlternativeSpine.tsv

Note that the path for the alternative file is relative to the module.

The data directory containing the bone mesh and landmark files must be in the same directory as the module.

****